Received: 29 November 2021 | Revised: 30 March 2022 | Accepted: 16 May 2022

DOI: 10.1002/eqe.3674

RESEARCH ARTICLE

WILEY

Within-event spatial correlation of peak ground acceleration and spectral pseudo-acceleration ordinates in the Chilean subduction zone

Sofía Aldea[1] | **Pablo Heresi**[1] | **César Pastén**[2]

[1]Departamento de Obras Civiles, Universidad Técnica Federico Santa María, Santiago, Chile

[2]Departamento de Ingeniería Civil, Facultad de Ciencias Físicas y Matemáticas, Universidad de Chile, Santiago, Chile

Correspondence
Pablo Heresi, Departamento de Obras Civiles, Universidad Técnica Federico Santa María, Santiago, Chile.
Email: pablo.heresi@usm.cl

Abstract

A regional seismic risk assessment requires the estimation of ground-motion intensities at multiple locations for a given event simultaneously. In this context, the spatial correlation of ground-motion residuals plays an important role in characterizing the probability distribution of the field of shaking intensities. Over the last 20 years, the spatial correlation of ground-motions has been widely studied and different models have been developed. In general, these models vary from each other depending on the ground-motion database used to generate them, on the adopted intensity measure, on the selected ground-motion model, and on the estimation methods, among others. This paper proposes a spatial correlation model for within-event residuals of peak ground acceleration and spectral pseudo-acceleration ordinates in the Chilean subduction zone. Although the database considered for this study has only a few well-recorded earthquakes, it contains a large number of station pairs sharing several common events. Therefore, we compute non-stationary correlations between station pairs and then fit a stationary spatial correlation model. Results of this paper are compared with previous models, concluding that, in general, subduction models show higher spatial correlations than those for active shallow crust events for long-period spectral ordinates. Moreover, no evidence was found for a systematic effect of earthquake magnitude or site conditions on spatial correlation. Finally, the proposed model is compared with a model obtained assuming stationarity in spatial correlations, showing more reliable estimates when using the proposed model.

KEYWORDS

Chilean subduction zone, ground-motion intensity measure, non-stationarity, regional seismic risk assessment, spatial correlation

1 | INTRODUCTION

Earthquakes can affect large regions of hundreds of kilometers, where hundreds or even thousands of structures are located. Thus, the estimation of the ground-motion intensities that can occur simultaneously at multiple sites during an earthquake is highly relevant when estimating the seismic performance of the threatened infrastructure and the potential seismic damage and losses. Generally, the mean and dispersion of ground-motion intensities for a given event can be estimated through ground-motion models (GMMs). However, in order to characterize the probability distribution of a

field (i.e., vector) of ground-motion intensity measures affecting several sites, the analyst needs not only information about the mean and dispersion, but also about the correlations of their residuals.[1,2]

The spatial correlation of residuals of ground-motion intensities has been extensively studied for the last 20 years.[3–31] In general, these studies combine several earthquakes for developing their models, although different authors have found a significantly large event-to-event variability,[12,23] even when exploring different events of the same seismic sequence.[26] Over the years, several researchers have studied different factors that might influence the spatial correlation. For example, site conditions and event magnitude influence on spatial correlations have been widely studied, showing discordant results within them.[14,18,23,25,26,30,31] Moreover, Goda and Atkinson[8,9] found larger spatial correlations for subduction earthquakes than those found by Jayaram and Baker[11] for active shallow crust events. More recently, the effects of the fitting method and spatial layout of the sites on the spatial correlation has been also examined.[24,26,27]

Most previous studies have used recordings of well-recorded events assuming stationarity when developing spatial correlation models.[7–11,13,15,16,19,21,23,24,29] This means that the semivariogram, and thus the correlation between residuals at two different sites, do not depend on the site locations, but only on their separation distance. With this assumption, different station pairs with a given separation distance can be used to estimate the semivariogram, which is useful when there is a lack of station pairs with several simultaneous recordings. Recent research has analyzed the influence of source and path effects in non-stationary correlations,[22,25,30] whereas Chen et al.[28] studied the non-stationary spatial correlation of ground-motions in New Zealand.

It is worth recalling that spatial correlation of ground-motion residuals may be primarily influenced by (a) earthquake source effects, (b) 3-D wave-propagation path from source to site and site-specific conditions, where sites with common wave-propagation paths due to similar geological conditions tend to present higher correlations, and (c) the relative position of near station pairs with respect to the main fault asperities, where stations with similar relative position tend to exhibit higher correlations.[6,22,26,28] Physical causes of non-stationarity in spatial correlations may be related to heterogeneous geological conditions, causing higher variations of spatial correlations,[28] beyond those that can be explained by only considering the separation distance as a determining variable. This is caused by the strong dependence of the 3-D propagation path and the frequency content of earthquake waves on the regional geological conditions.[15] On the other hand, spatial correlations can also be affected by bias in GMMs. Some bias could be produced by differences in the site-characterization parameter values used to define the GMM and the ones in the data set used for computing spatial correlations. The most common site-characterization parameter used in GMMs is the time-averaged shear-wave velocity to 30 meters depth of soil, V_{S30}. Accordingly, if the GMM is not well-defined for a specific range of V_{S30} values, the misfit in the ground-motion estimation for that range of V_{S30} will eventually impact spatial correlations, increasing their value. Regarding the effect of moment magnitude on correlations, results from several studies[14,18,30] show that the spatial correlation tends to increase with increasing earthquake magnitude. In particular, for moderate-to-large earthquakes, an additional non-random component in the residuals has been identified, resulting in relatively higher levels of ground-motion correlation. This non-random component of the residuals might be related to low-frequency content generated by moderate-to-large earthquakes.[30] However, a number of researchers[11,23,31] did not find any statistically significant relationship between earthquake magnitude and spatial correlation.

In this context, this paper presents a spatial correlation model for within-event residuals of peak ground acceleration (PGA) and 5%-damped spectral pseudo-acceleration ordinates at different periods of vibration (Sa(T)) in the Chilean subduction zone. The Chilean seismic network has recorded a large number of common events in different pairs of stations. Therefore, the assumption of stationarity can be skipped in this case. Thus, we compute non-stationary empirical correlations between station pairs at different separation distances, and then a stationary exponential spatial correlation model is fitted for its general use. Then, we compare the proposed spatial correlation model against previously developed models. Furthermore, we analyze the influence of earthquake magnitude and site conditions on the spatial correlation model, finding no evidence of a systematic effect for either of these variables. Finally, a comparison between the proposed model and a model fitted from empirical correlations computed using the standard approach of assuming stationarity in spatial correlations is performed, finding better estimations for the proposed model in terms of the standard errors of the estimators.

2 | GROUND-MOTION DATABASE

For this study, we used the ground-motion database compiled by Bastías and Montalva,[32] which contains 3572 records in the three perpendicular directions at 181 stations, from 477 events. These events were recorded between March 1985

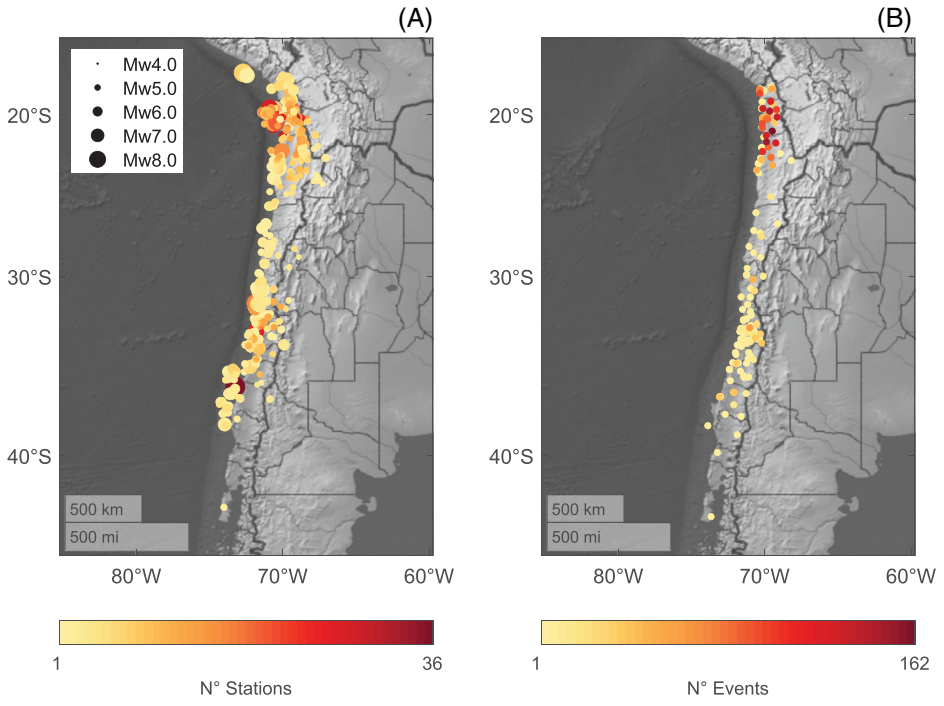

FIGURE 1 (A) Geographical location of the epicenters of the 469 earthquakes in the selected database of this study, along with the number of stations that recorded each event. (B) Geographical location of the 181 strong-motion stations in the selected database of this study, along with the number of events recorded by every station

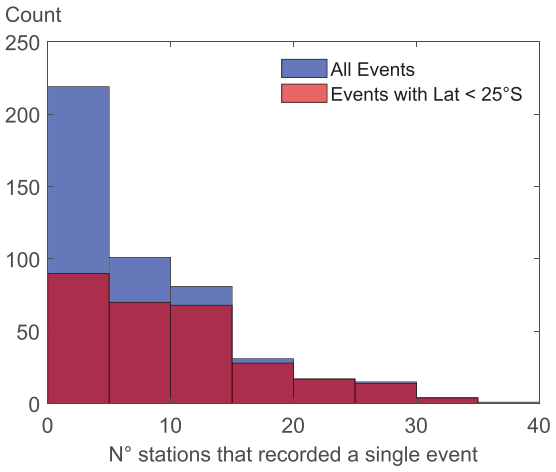

FIGURE 2 Histogram of the number of strong-motion stations that recorded each earthquake

and September 2015 in Chile. We selected 469 interface and intraslab events for the analysis: 278 interface earthquakes with moment magnitudes ranging between M_w4.6 and M_w8.8 (including the Mw8.8 2010 Maule Earthquake), and 191 intraslab earthquakes with moment magnitudes varying between M_w4.6 and M_w7.8 (including the M_w7.8 2005 Tarapacá Earthquake). The database has information on the V_{S30}, rupture distance, R_{rup}, and hypocentral distance, R_{hyp} of all the recordings.

The geographical distribution of the 469 selected events is shown in Figure 1(A), which also illustrates the moment magnitude and the number of stations that recorded each event. Figure 1(B) presents the geographical distribution of the 181 strong-motion stations of the database, along with the number of events recorded by each station. A histogram of the number of stations per event is shown in Figure 2. In this figure, it is noticed that most of the events were recorded by less than 20 stations. In Figure 2, the M_w8.8 2010 Maule Earthquake is the one with the greatest number of recording stations:

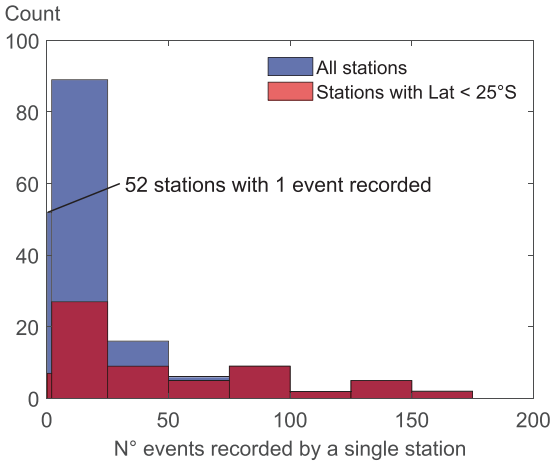

FIGURE 3 Histogram of the number of events recorded by each strong-motion station

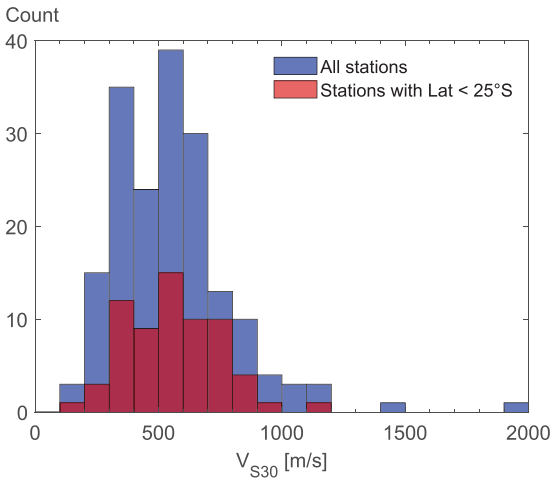

FIGURE 4 Histogram of the time-averaged shear-wave velocity to 30 meters depth of soil, V_{S30}, at the site of every strong-motion station

36. Moreover, only 37 events (8% of the total number of events) have 20 or more recording stations, and 35 of these 37 events have their recording stations in the northern region of the country (Lat < 25°S).

Due to a lack of well-recorded events in the Chilean database (all the events were recorded by fewer than 37 stations), it is not possible to fit spatial correlation models to individual events to consider the event-to-event variability, as performed by Goda[12] and Heresi and Miranda.[23] This is because the reliability of the empirical correlations increases with the number of recording stations of the earthquake. However, there is something relevant to notice from Figure 1(B). It is observed that there are several stations with a considerable number of recorded events (24 stations have recorded more than 50 events), especially in the northern region of the country. This can also be seen in Figure 3, which shows a histogram of the number of events recorded per station, showing that 24 stations have more than 50 events recorded. In particular, 23 of these 24 stations are located in the northern region of Chile (Lat < 25°S).

A histogram of the V_{S30} of each station is presented in Figure 4, where most of the stations present a V_{S30} between 300 and 700 m/s. Moreover, no significant distribution differences are observed between the V_{S30} values of stations in the northern region of Chile (Lat < 25°S) and the rest of the country.

From Figure 1(B) and Figure 3, it is inferred that if there are several stations with more than 50 events recorded and most of them are in the northern region of Chile, there should be several pairs of stations that share a large number of common events. Thus, Figure 5 presents the number of common recorded events as a function of the separation distance of all the possible pairs of stations. Consequently, the procedure adopted in this study is to compute non-stationary empirical correlations of a set of selected pairs of stations with separation distances ranging between 1 and 300 km. We selected a total of 42 station pairs with the largest possible number of common recorded events at different separation distances,

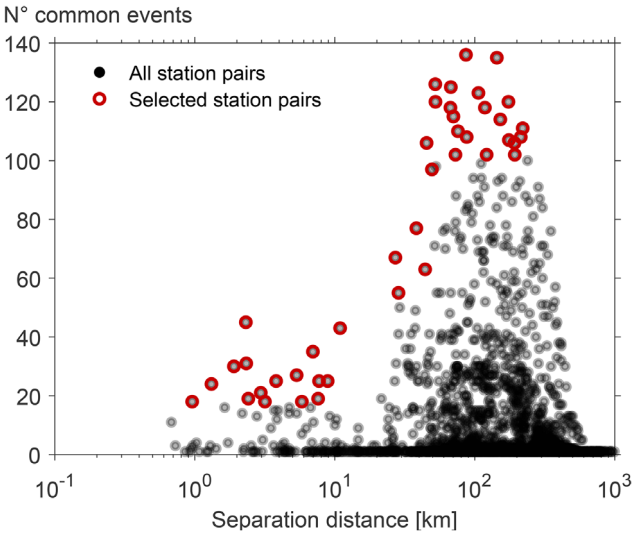

FIGURE 5 Separation distance and number of events recorded simultaneously in every pair of strong-motion stations. A total of 42 station pairs were selected for this study

as shown with red circles in Figure 5. The choice is such that, for separation distances less than 15 km, the number of common events must be greater than 18; for distances between 15 and 50 km, the number of common events must be greater than 50; and for distances greater than 50 km, the number of common events must be greater than 100. The basis for selecting a different minimum of stations for each distance range is defined in order to get reliable results, due to the sparse information for Chilean subduction records.

3 | GROUND-MOTION SPATIAL CORRELATION MODEL

Ground-motion intensities can be typically characterized by lognormally distributed random variables[33,34] and GMMs estimate their medians and dispersions as a function of the event magnitude M, source-to-site distance R, and a set of other causal parameters θ (i.e., other source and site characteristics). For this study, the GMM developed by Montalva et al.[35] for the Chilean subduction zone is used. To this extent, the GMM used in this study was constructed employing the same database that we are using in this instance to compute empirical spatial correlations. Thus, bias in V_{S30} scaling may be minimized. Equation (1) expresses the formulation for estimating the ground-motion intensity at a given site:

$$\ln IM_{sr} = \mu\left(IM,\ M_r, R_{sr}, \boldsymbol{\theta_{sr}}\right) + \delta B_r\left(IM\right) + \delta W_{sr}\left(IM\right) \tag{1}$$

where IM_{sr} is the observed value of the ground-motion intensity measure (in this study, PGA or Sa(T)) at the s-th site during the r-th earthquake rupture and $\mu(IM,\ M_r, R_{sr}, \boldsymbol{\theta_{sr}})$ is the predicted mean value of its logarithm obtained through the GMM. The randomness of the intensity measure is characterized by the between- and within-event residual terms, $\delta B_r(IM)$ and $\delta W_{sr}(IM)$, respectively. The between- and within-event residual terms are assumed to be independent of each other and normally distributed with zero mean and standard deviations $\tau(IM)$ and $\phi(IM)$, respectively. Note that $\mu(IM,\ M_r, R_{sr}, \boldsymbol{\theta_{sr}})$, $\delta B_r(IM)$, $\delta W_{sr}(IM)$, $\tau(IM)$ and $\phi(IM)$ depend on the considered intensity measure, IM. Moreover, the between-event residual $\delta B_r(IM)$ does not depend on the site characteristics, but only on the rupture, therefore it is common for all sites for a given event.

We compute the maximum likelihood estimate of the between-event residual for event r, $\widehat{\delta B}_r(IM)$, through Equation (2),[36] where n_r is the number of recordings of event r:

$$\widehat{\delta B}_r\ (IM) = \frac{\sum_{s=1}^{n_r}\left(\delta B_r\left(IM\right) + \delta W_{sr}\left(IM\right)\right)}{\frac{\phi(IM)^2}{\tau(IM)^2} + n_r} = \frac{\sum_{s=1}^{n_r}\ln IM_{sr} - \mu\left(IM,\ M_r, R_{sr}, \boldsymbol{\theta_{sr}}\right)}{\frac{\phi(IM)^2}{\tau(IM)^2} + n_r} \tag{2}$$

Then, we estimate the normalized within-event residuals at two different sites, i and j, during the event r, $\widetilde{\delta W}_{ir}(IM)$ and $\widetilde{\delta W}_{jr}(IM)$, respectively, through Equation (3) and Equation (4):

$$\widetilde{\delta W}_{ir}\ (IM) = \frac{\widehat{\delta W}_{ir}\,(IM)}{\phi\,(IM)} = \frac{\ln IM_{ir} - f\,(IM,\ M_r, R_{ir}, \boldsymbol{\theta_{ir}}) - \widehat{\delta B}_r\,(IM)}{\phi\,(IM)} \tag{3}$$

$$\widetilde{\delta W}_{jr}\ (IM) = \frac{\widehat{\delta W}_{jr}\,(IM)}{\phi\,(IM)} = \frac{\ln IM_{jr} - f\left(IM,\ M_r, R_{jr}, \boldsymbol{\theta_{jr}}\right) - \widehat{\delta B}_r\,(IM)}{\phi\,(IM)} \tag{4}$$

Finally, we compute the empirical Pearson's correlation coefficient to quantify the spatial correlation between the normalized within-event residuals $\widetilde{\delta W}_{ir}(IM)$ and $\widetilde{\delta W}_{jr}(IM)$ at selected pairs of sites within the Chilean strong-motion network, since it can represent a non-stationary and anisotropic behavior. At this point, it is important to notice that this approach requires simultaneous observations of the intensity measure of interest at both sites for multiple earthquakes. Thus, we use the pairs of stations selected in the previous section (see Figure 5), which have more than 17 common recorded events and separation distances ranging between 1 and 300 km.

After computing the empirical Pearson's correlation coefficient between the selected pairs of stations at different separation distances, we fit the following exponential model, expressed in Equation (5):

$$\hat{\rho}_W\ (\Delta, IM) = \exp\left[-\left(\frac{\Delta}{\beta\,(IM)}\right)^{\alpha(IM)}\right] \tag{5}$$

where Δ is the separation distance between the sites, and α and β are the model parameters, which in turn depend on the considered ground-shaking intensity measure. In Equation (5), α is a unitless parameter that defines the rate of decay of the spatial correlation with Δ, whereas β is the distance, in km, at which the spatial correlation reaches a value of exp(-1) = 0.368. In order to determine α and β, a weighted least-squares regression was performed on the transformed values of spatial correlation, using the Fisher z transformation, as follows in Equation (6):

$$z\ = \frac{1}{2}\ \log\left(\frac{1+\rho}{1-\rho}\right) \tag{6}$$

where ρ is the empirical Pearson's correlation between a pair of stations and z is its transformed value. The weight factor of each data point in the weighted least squares is n_{ij}-3, where n_{ij} is the number of common events recorded at stations i and j simultaneously. Note that this weight factor corresponds to the reciprocal of the variance of z.

4 | SPATIAL CORRELATION OF WITHIN-EVENT RESIDUALS

The spatial correlation model of Equation (5) was fitted to the empirical correlations of selected pairs of stations as previously specified, using the peak ground acceleration (PGA) and spectral pseudo-acceleration ordinates at 19 periods of vibration between 0.1s and 10s as the intensity measure of interest. For example, Figure 6 shows the fitted spatial correlation model (Fisher z transformation) for Sa(1s), where $\alpha = 0.70$ and $\beta = 13.5$ km. The shaded blue area represents the 95% confidence interval of the regression fit.

In order to simplify the proposed spatial correlation model, a fixed value of α is considered for the entire period range. Figure 7 illustrates how the mean squared error (MSE), averaged among the weighted regressions performed for all the intensity measures of interest, varies when using a fixed value of α, as opposed to fitting a different α value for every regression. The minimum average MSE, which is reached when $\alpha = 0.59$, is just 2.8% greater than the average MSE obtained when fitting an α value for each intensity measure (shown in Figure 7 as "MSE for variable α"). Therefore, we use $\alpha = 0.59$ for the spatial correlation model of all the considered intensity measures. Note that this value is similar to the one obtained by Heresi and Miranda,[23] who used recordings from active shallow crust regions. Furthermore, a smoothing of the model parameter β is performed, as shown in Figure 8. With these assumptions, the proposed spatial correlation model is then expressed in Equation (7), while Table 1 presents the unsmoothed and smoothed β values for PGA and Sa(T) at periods

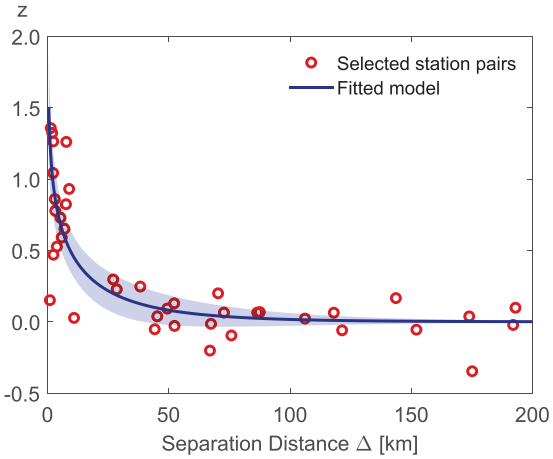

FIGURE 6 Fisher z transformation of empirical correlations and fitted spatial correlation model for Sa(1s). The shaded area represents the 95% confidence interval of the regression fit ($\alpha = 0.70$ and $\beta = 13.5$ km)

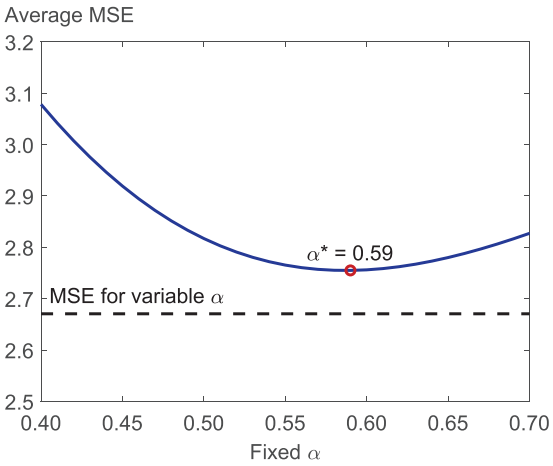

FIGURE 7 Variation of MSE averaged among all the considered intensity measures when fitting spatial correlation models with a fixed α as opposed to spatial correlation models with variable α.

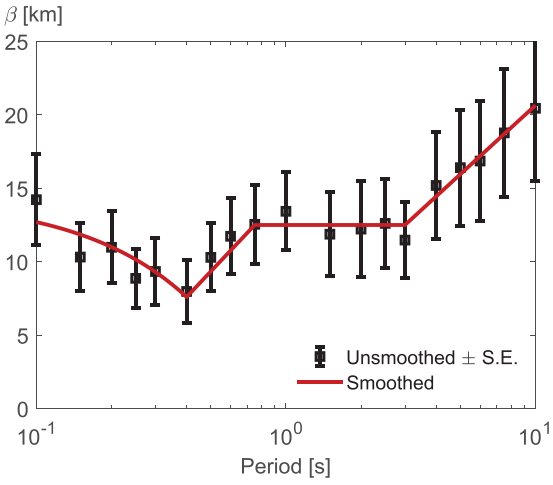

FIGURE 8 Smoothing of model parameter β

TABLE 1 Model parameter β and its standard error (S.E.), as a function of the intensity measure of interest

Intensity measure	Unsmoothed β [km]	S.E. of β [km]	Smoothed β [km]
PGA	14.42	3.4	14.40
Sa(0.1s)	14.22	3.1	12.70
Sa(0.15s)	10.32	2.3	11.85
Sa(0.2s)	10.98	2.4	11.00
Sa(0.25s)	8.87	2.0	10.15
Sa(0.3s)	9.34	2.3	9.30
Sa(0.4s)	7.98	2.1	7.60
Sa(0.5s)	10.30	2.3	9.34
Sa(0.6s)	11.73	2.6	10.76
Sa(0.75s)	12.55	2.7	12.50
Sa(1s)	13.43	2.7	12.50
Sa(1.5s)	11.87	2.9	12.50
Sa(2s)	12.22	3.3	12.50
Sa(2.5s)	12.61	3.0	12.50
Sa(3s)	11.47	2.6	12.50
Sa(4s)	15.19	3.6	14.45
Sa(5s)	16.40	4.0	15.96
Sa(6s)	16.85	4.1	17.19
Sa(7.5s)	18.77	4.3	18.70
Sa(10s)	20.45	4.9	20.65

between 0.1s and 10s. Smoothed values of β follow a piecewise-defined function, as stated in Equation (8).

$$\hat{\rho}_W\ (\Delta, IM) = \exp\left[-\left(\frac{\Delta}{\beta\,(IM)}\right)^{0.59}\right] \tag{7}$$

$$\beta\ [km] = \begin{cases} 14.400 - 17.000 \cdot T & T \leq 0.40s \\ 14.743 + 7.795 \cdot \ln(T) & 0.40s < T \leq 0.75s \\ 12.500 & 0.75s < T \leq 3.00s \\ 5.063 + 6.769 \cdot \ln(T) & 3.0s < T \leq 10.0s \end{cases} \tag{8}$$

Figure 9 shows a comparison between the spatial correlation model proposed in this study against the models previously developed by Jayaram and Baker[11] [JB2009], Goda and Atkinson[8] [GA2009], Goda and Atkinson[9] [GA2010], Esposito and Iervolino[13] [EI2012] and by Heresi and Miranda[23] [HM2019]. The comparison is performed for PGA, Sa(1s), Sa(2s) and Sa(5s). 16th and 84th percentiles from HM2019 are represented as pink shaded areas. It is observed that the proposed spatial correlation model for short to medium vibration periods is, in general, similar to the median of the HM2019 model. On the other hand, for longer periods (e.g., T = 5s), the proposed spatial correlation model is higher than the median of the HM2019 model and closer to the GA2009 and GA2010 models, which were developed for Japanese subduction earthquakes. The large spatial correlations of long-period spectral ordinates observed in this study are also in accordance with the findings of Candia et al.,[37] who used a ground-motion database of Chilean earthquakes to develop inter-period correlations of spectral ordinates and found larger correlations than those previously obtained for active shallow crust regions. However, inter-period correlations depend on the frequency content of earthquake ground-motions at a specific site,[37] while spatial correlations are associated to the wave propagation path from source to site, local site effects, and relative location to main fault asperities.[6] Thus, higher values of inter-period correlations do not necessary indicate higher values of spatial correlations.

A reason for higher spatial correlations for long-period spectral ordinates in Chilean data, in comparison with other regions, is still unknown and could be hypothesized to be due to the relative size of the events in subduction and active

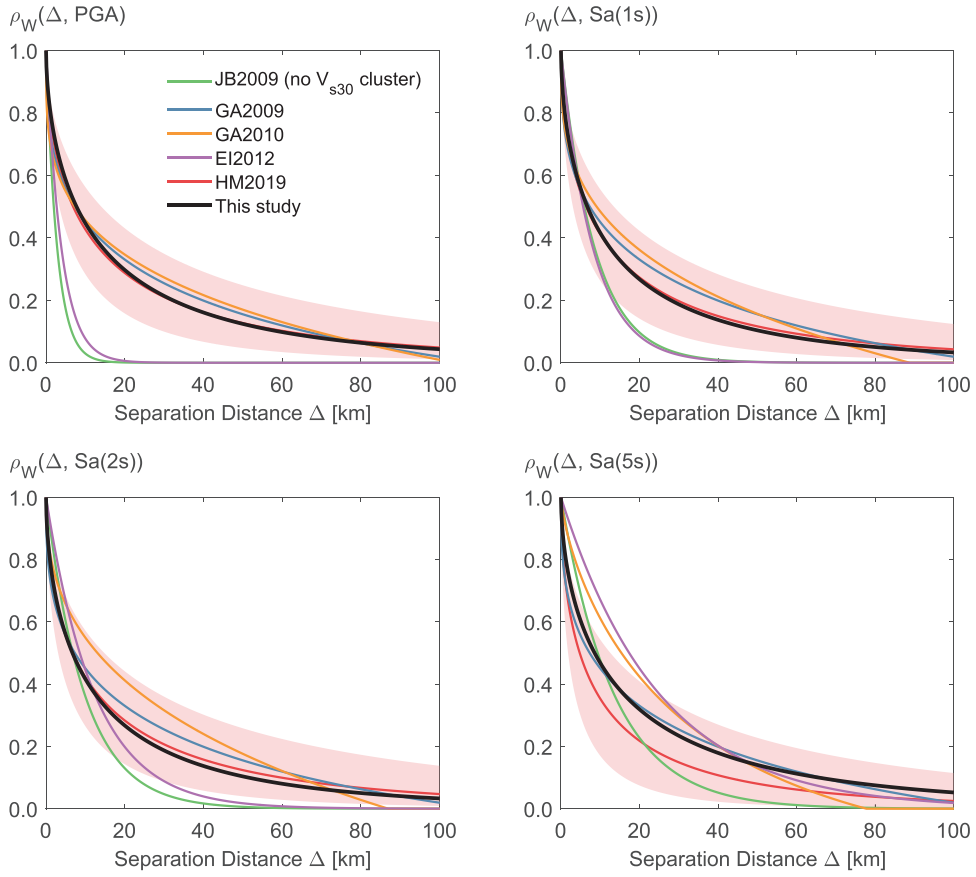

FIGURE 9 Comparison of the proposed spatial correlation model for PGA and Sa(T) at vibration periods of 1s, 2s, and 5s against previously developed models. JB2009: Jayaram and Baker 2009[11]; GA2009: Goda and Atkinson 2009[8]; GA2010: Goda and Atkinson 2010[9]; EI2012: Esposito and Iervolino 2012[13]; HM2019: Heresi and Miranda 2019.[23] Pink shaded areas represent the 16th/84th percentiles from HM2019.[23]

FIGURE 10 Comparison of the range (i.e., distance at which the spatial correlation decays to exp(-3)) of Sa(T) of different spatial correlation models

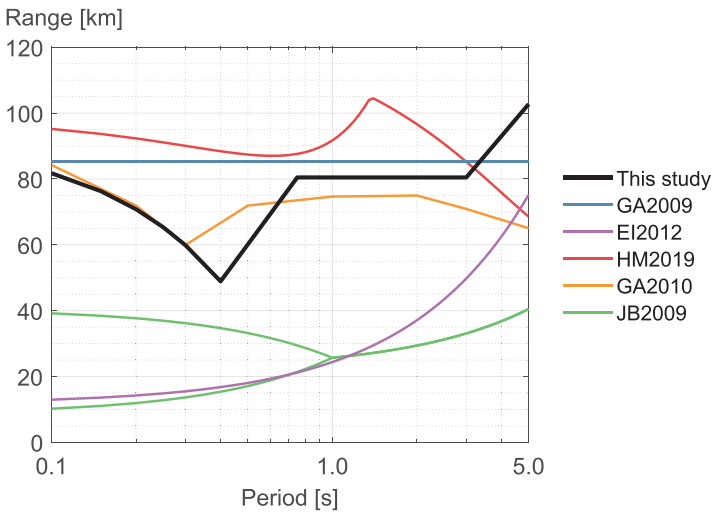

shallow crust tectonic regions. Therefore, we will further study the influence of the event magnitude in the empirical spatial correlations in a subsequent section.

Figure 10 shows the range (i.e., separation distance at which the spatial correlation model of within-event residuals decays to exp(-3)) for Sa(T) as a function of the vibration period. In this study, the range has a value of 82 km for T = 0.1s and decreases rapidly with increasing vibration period up to T = 0.4s, a period at which the range begins to increase.

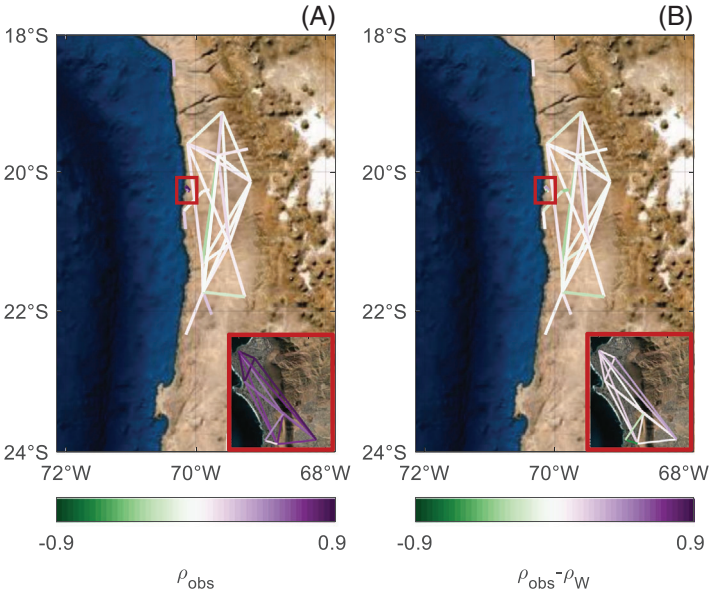

FIGURE 11 (A) Map of empirical (observed) spatial correlations between the selected station pairs for Sa(1s). (B) Map of the difference between the empirical (observed) correlation and the estimated correlation using the proposed exponential model between the selected station pairs for Sa(1s). Insets present an amplification for latitudes between 20.29°S and 20.20°S (red boxes)

Overall, results of this study are consistent with the results obtained by GA2009, GA2010 and HM2019. On the other hand, it is noticed that JB09 and EI2012 models lead to significantly lower ranges for periods shorter than 3s.

The increase in the range with the period, for periods higher than 0.4s, is in agreement with findings of previous studies,[11,13,30] and is consistent with past research about ground-motion coherency.[38] Coherency is a measure of correlation between two time series (in this case, spatially separated ground-motion time series). Generally speaking, coherency decreases due to the dispersion of waves during propagation, with larger reduction for high-frequency waves, since these waves tend to be more influenced by small-scale heterogeneities in the propagation path because of their shorter wavelengths.[39] Accordingly, high-frequency waves tend to be less coherent than low-frequency waves.[38] Considering the last, it is logical to expect more correlated residuals of peak amplitudes for long periods than for short periods, which is consistent with the period dependence of the range.

Finally, maps of correlation estimates are considered in order to identify any spatial pattern of the spatial correlation that could be related to the 3-D crustal structure. In Figure 11(A) we plot maps of the individual empirical spatial correlations (ρ_{obs}) within the selected station pairs, for Sa(1s), while in Figure 11(B), we plot maps of the differences between the empirical spatial correlations (ρ_{obs}) and the estimation through the proposed exponential model (ρ_W), $\rho_{obs} - \rho_W$, for Sa(1s). The respective values are color-scaled in the maps. No clear spatial pattern is identified in Figure 11(A) and in Figure 11(B). The same conclusion can be drawn from similar maps of spatial correlations of other intensities.

5 | EFFECT OF THE MOMENT MAGNITUDE

The effect of the event moment magnitude in the non-stationary empirical correlations is studied in this section. For each pair of stations, through Equation (9), we perform the following regression:

$$\widetilde{\delta W}_{jr}\ (IM) = \gamma_0\ + \gamma_1 \cdot \widetilde{\delta W}_{ir}\,(IM) + \gamma_2 \cdot (M_r - 5.5) \cdot \widetilde{\delta W}_{ir}\,(IM) \tag{9}$$

In Equation (9), γ_2 measures the effect of the event magnitude on the correlation between $\widetilde{\delta W}_{ir}$ and $\widetilde{\delta W}_{jr}$. In this context, a $\gamma_2 > 0$ means that higher magnitudes lead to higher correlations, whilst a $\gamma_2 < 0$ means that higher magnitudes are related to lower correlations. Figure 12 shows a histogram of γ_2 values for different station pairs, at a vibration period of 2s. In this figure, the total number of station pairs sums 42, corresponding to the 42 selected pairs of stations (see Figure 5), while red and green bars represent the number of station pairs where regressions from Equation (9) present a p-value of γ_2 lower than 0.05, and thus are deemed to be statistically significant. For this period of vibration, it can be seen that the regression in six station pairs resulted in a $\gamma_2 > 0$ with a p-value lower than 0.05, whereas the regression in four station pairs resulted in a $\gamma_2 < 0$ with a p-value lower than 0.05. The regression in the remaining 32 station pairs resulted in a γ_2 that is not statistically significant, meaning no evidence of an effect of the event moment magnitude in the correlation

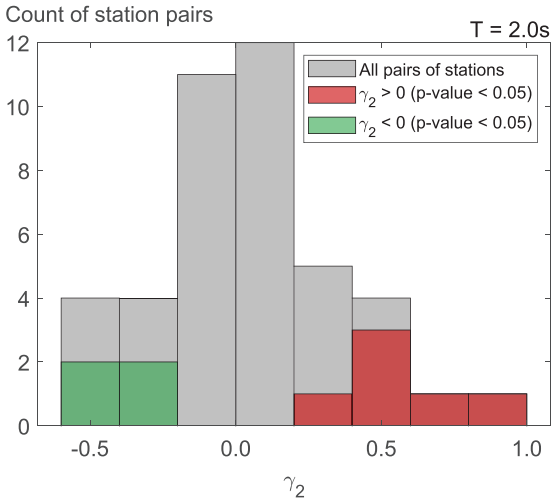

FIGURE 12 Histogram of γ_2 for Sa(2s), computed from regressions at different station pairs. Six out of the 42 station pairs (14.3%) present a statistically significant $\gamma_2 > 0$, whereas four out of the 42 station pairs (9.5%) present a statistically significant $\gamma_2 < 0$

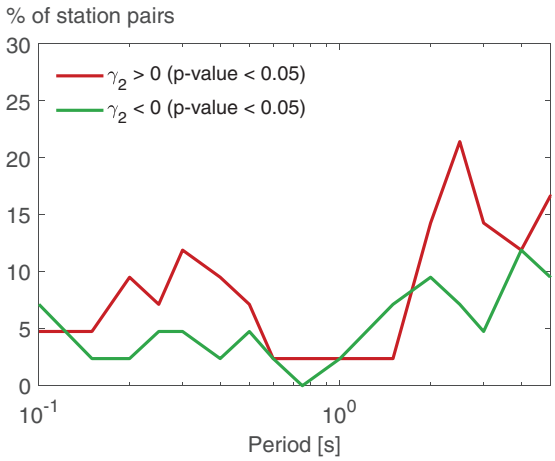

FIGURE 13 Percentage of stations with statistically significant $|\gamma_2| > 0$ for all the considered ground-motion intensity measures

between $\widetilde{\delta W}_{ir}$ and $\widetilde{\delta W}_{jr}$. We repeated this procedure and obtained the percentage of station pairs in which $\gamma_2 > 0$ and $\gamma_2 < 0$ (both with p-value < 0.05), which is shown in Figure 13. We observe that the percentages of station pairs with a statistically significant γ_2 are lower than 25% for all the considered ground-shaking intensity measures. Furthermore, there is no systematic dominance of station pairs with $\gamma_2 > 0$ over those with $\gamma_2 < 0$ or vice versa. Therefore, there is not enough evidence for rejecting the hypothesis that there is not a systematic effect of event magnitude on the non-stationary empirical spatial correlations. These results are consistent with the findings of Heresi and Miranda[23] and Schiappapietra and Douglas.[26]

The last results could be related with the frequency-dependence to the spatial distribution of seismic radiation in subduction earthquakes (e.g., Valparaíso 1985, Maule 2010, Tokohu 2011), studied previously by several authors.[40–42] These studies have demonstrated that high-frequency (e.g., > 1 Hz) sources are associated with regions that presented strong seismic coupling on the fault prior to the earthquake, while low-frequency (e.g., < 0.2 Hz) sources are located around the epicenter. These regions of strong coupling might be more heterogenous and/or have higher stress levels, and, consequently, be more probable to generate higher frequency radiation. Therefore, it is inferred from these studies that high-frequency (short period) waves are associated with the size of the asperities rather than moment magnitude. Consequently, spatial correlation of ground-motion intensities at high frequencies would also be related to the properties of the asperities rather than to earthquake magnitude.

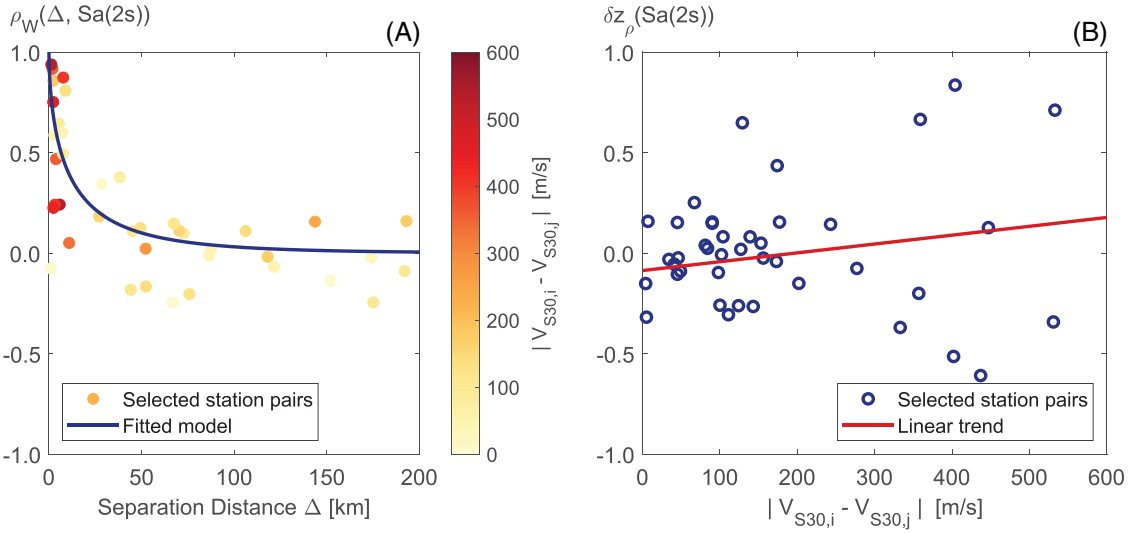

FIGURE 14 (A) Observed and fitted spatial correlation values as a function of the separation distance, for Sa(2s). Each point presents the difference in the V_{S30} values of both stations. (B) Observed correlations with respect to the model as a function of the difference in the V_{S30} values for each pair of stations, for Sa(2s)

6 | EFFECT OF SITE CONDITIONS

The influence of the local site conditions in spatial correlations is analyzed in this section, specifically the effect of V_{S30}. First, we define δz_p as follows in Equation (10):

$$\delta z_p = z_{obs} - z_{model} \tag{10}$$

where z_{obs} and z_{model} are the observed and predicted values of the Fisher z transformation of the spatial correlation between an IM at a pair of stations. Therefore, if a station pair has a value of $\delta z_p > 0$, that station pair has a higher observed correlation than the one estimated by the model for their separation distance. On the other hand, if a station pair has a value of $\delta z_p < 0$, that station pair has a lower observed correlation than the one estimated by the model for their separation distance.

In order to evaluate whether the similarity or disparity between the local site conditions at a pair of stations has an effect in their spatial correlation, we will evaluate the hypothesis that the station pairs with higher correlations with respect to the model (i.e., $\delta z_p > 0$) are the ones that present similar values of V_{S30}, while station pairs with lower correlations with respect to the model (i.e., $\delta z_p < 0$), are the ones with the highest differences in their V_{S30}. This hypothesis is based on the premise that in pairs of stations with larger differences in their V_{S30} values, one of them may be located on a softer soil, probably on basins with strong 3-D effects, decreasing spatial correlation between both sites.

Figure 14(A) shows the observed spatial correlations for Sa(2s) of the selected station pairs and the fitted model, along with their difference between V_{S30} values. Figure 14(B) presents the δz_pvalues for Sa(2s) as a function of the difference between V_{S30} values, for each station pair. Furthermore, in Figure 14(B) a linear trend was fitted through a weighted regression to the data points, which results in a slope, γ_{Vs30}, of 0.00044. As observed in Figure 14, there is no evidence of a relationship between large δz_p values and low $|V_{S30,i} - V_{S30,j}|$. Furthermore, for this particular IM the trend between δz_p and the difference in V_{S30} is the opposite than the one expected. In addition, the p-value for γ_{Vs30} is equal to 0.192, concluding that, for this IM, γ_{Vs30} is not statistically significant for a significance level of 5%.

We repeated the same procedure described above for each of the IMs considered in this study. Figure 15 shows γ_{Vs30} and its p-value as a function of the IM, where, for most of the cases, the p-value is greater than 5%. This result shows that there is not enough evidence for rejecting the hypothesis that the difference between V_{S30} values at both stations does not have a statistically significant effect in their spatial correlations. In other words, we cannot refuse that the spatial correlation of an IM between two stations is not affected by the differences in their local site conditions, measured through their V_{S30}. This inconsistency with respect to the hypothesis may occur since there are no stations, in the analyzed database, located

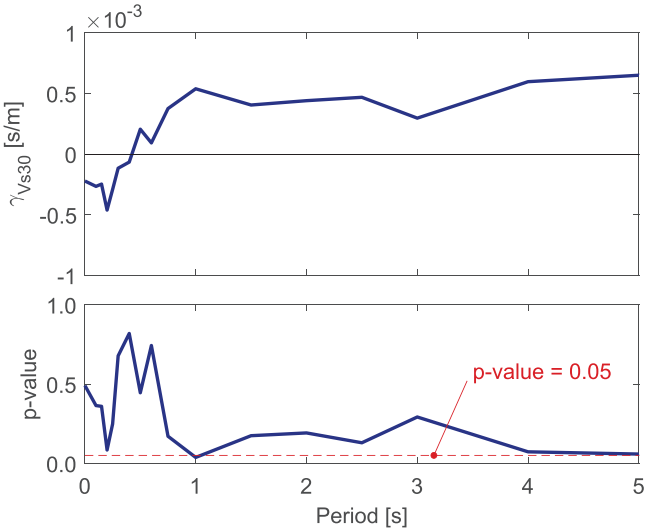

FIGURE 15 γ_{Vs30} and its *p*-value as a function of the considered IM. For most of the cases, the *p*-value is greater than 5%, and therefore γ_{Vs30} is not statistically significant for a significance level of 5%

on sites with such lower values of V_{S30}, which account for basin effects. Nevertheless, this finding is consistent with the results obtained by Heresi and Miranda[23] for shallow crust earthquakes.

7 | COMPARISON BETWEEN THE PROPOSED APPROACH AND A STANDARD APPROACH

We performed a comparison between the previously proposed non-stationary approach and a standard approach that assumes stationarity in the calculation of empirical correlations. For the standard approach, within-event residuals from different station pairs with a given separation distance can be used to estimate the semivariogram and, in consequence, spatial correlations, as stated in Equation (11). It is worth noting that this assumption does not consider exact values of separation distances but organizes them in bins of distances. In Equation (11), for a given IM, $\rho_W(\Delta, IM)$ denotes the "observed" spatial correlation for a particular bin of separation distance Δ, while $\phi_d(\Delta, IM)$ represents the standard deviation of the difference between residuals at pairs of stations within a bin of separation distance Δ. $\hat{\phi}(IM)$ is assumed as $\phi_d(\Delta, IM)\sqrt{0.5}$ for a very large separation distance[23] (e.g., $\geq 100km$).

$$\rho_W(\Delta, IM) = 1 - \frac{(\phi_d(\Delta, IM))^2}{2\left(\hat{\phi}(IM)\right)^2} \tag{11}$$

Afterwards, the spatial correlation model from Equation (5) is fitted to the observed correlation values, estimated through the standard approach, by following the same procedure proposed for non-stationary correlations.

A comparison between both approaches is then presented in Figure 16, for Sa(5s). Figure 16 shows similar mean values for both approaches, but a clearly wider 95% confidence interval for the standard approach. Furthermore, Table 2 presents the standard errors of the model parameters α and β obtained from both approaches, for PGA, Sa(1s), Sa(2s) and Sa(5s), showing a reduction of approximately 50% of the error when considering the proposed non-stationary approach. Thus, it is concluded that the proposed approach provides more reliable models than the standard approach.

8 | CONCLUSIONS

In this study, we propose a within-event spatial correlation model for peak ground acceleration and spectral pseudo-acceleration ordinates in the Chilean subduction zone. Chile has had several seismic events within a wide range of moment magnitudes, with the largest recorded event being the 2010 M_w8.8 Maule earthquake, but only a few ground-motion

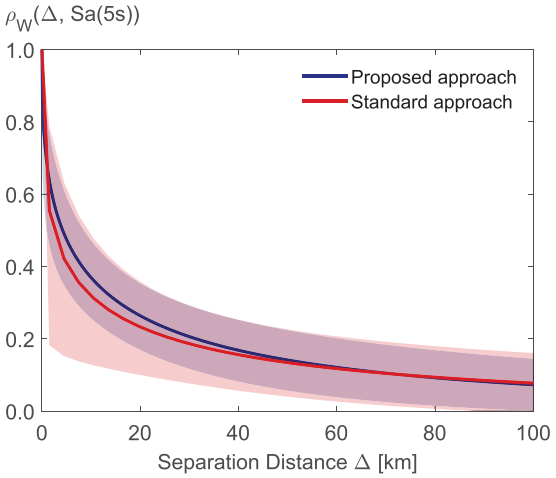

FIGURE 16 Comparison of the proposed spatial correlation model for Sa(5s) and a model developed using a standard approach. Shaded areas represent the 95% confidence interval of each model

TABLE 2 Reduction of the standard error of model parameters when using the proposed approach to develop spatial correlation models

	Standard error of α		Standard error of β [km]	
Intensity measure	**Standard approach**	**Proposed approach**	**Standard approach**	**Proposed approach**
PGA	0.17	0.08	6.74	3.84
Sa(1s)	0.71	0.07	11.45	3.60
Sa(2s)	0.10	0.07	3.90	2.67
Sa(5s)	0.11	0.07	4.43	2.77

records per event have been recorded. However, there are several pairs of stations that have recorded a large number of earthquakes simultaneously. Therefore, a non-stationary empirical correlation between pairs of stations at different separation distances can be computed through the Pearson's correlation coefficient.

We fitted an exponential model that decays with increasing separation distance to the empirical values of spatial correlation, whose model parameters depend on the considered ground-shaking intensity measure. Results of this model show that the spatial correlations of spectral pseudo-acceleration ordinates are close to the median of Heresi and Miranda[23] for periods shorter than 2s. On the other hand, for longer periods, the proposed model is closer to the values proposed by Goda and Atkinson,[8,9] which shows higher spatial correlations for subduction earthquakes than those for active shallow crust events. Furthermore, we studied the effect of the event moment magnitude on the non-stationary empirical spatial correlations, showing that there is no evidence of a systematic effect of magnitude on the spatial correlation. Additionally, we analyzed the influence of the differences of local site conditions in spatial correlations, concluding that the difference between the V_{S30} values at both stations does not present a statistically significant contribution to the spatial correlations estimated by the model. We finally performed a comparison between the results obtained with the proposed non-stationary approach, with those obtained with a standard approach that assumes stationarity in spatial correlations, finding significantly lower estimation errors when considering the proposed approach.

Although we computed non-stationary empirical correlations between specific station pairs within Chile, the proposed spatial correlation model can be extended for any pair of sites within the country. The novel approach of this article, however, does not allow us to estimate an event-to-event variability in the spatial correlation model, as did in previous studies.[12,23] The proposed spatial correlation model for the Chilean subduction zone can be used for estimating ground-shaking intensity measures at several sites simultaneously in order to perform regional seismic hazard and regional seismic risk evaluations.

ACKNOWLEDGMENTS

The authors would like to acknowledge the financial support of FONDECYT Project N°3200924. The authors are grateful to the Chilean National Seismological Center (CSN) and the National Network of Accelerometers of the Department of Civil Engineering of the University of Chile (RENADIC) for the installation and maintenance of strong-motion seismic

stations and for making their data publicly available, and to Bastías and Montalva[32] for gathering, processing, and distributing these recordings. Finally, the authors would like to acknowledge Dr. Norman Abrahamson and an anonymous reviewer for their valuable comments and suggestions that significantly improved the quality of this article.

DATA AVAILABILITY STATEMENT

The data that support the findings of this study are available from the corresponding author upon reasonable request.

ORCID

Sofia Aldea https://orcid.org/0000-0001-8162-3450
Pablo Heresi https://orcid.org/0000-0003-4594-0621
César Pastén https://orcid.org/0000-0002-6683-0619

REFERENCES

1. Wesson R, Perkins D. Spatial correlation of probabilistic earthquake ground motion and loss. *Bull Seismol Soc Am*. 2001;91(6):1498-1515.
2. Lee R, Kiremidjian A. Uncertainty and correlation for loss assessment of spatially distributed systems. *Earthq Spectra*. 2007;23(4):753-770.
3. Boore D. Estimated ground motion from the 1994 Northridge, California, earthquake at the site of the Interstate 10 and La Cienega Boulevard bridge collapse, West Los Angeles, California. *Bull Seismol Soc Am*. 2003;93(6):2737-2751.
4. Kawakami H, Mogi H. Analyzing spatial intraevent variability of peak ground accelerations as a function of separation distance. *Bull Seismol Soc Am*. 2003;93(3):1079-1090.
5. Wang M, Takada T. Macrospatial correlation model of seismic ground motions. *Earthq Spectra*. 2005;21(4):1137-1156.
6. Park J, Bazzurrro P, Baker J. Modeling spatial correlation of ground motion intensity measures for regional seismic hazard and portfolio loss estimation. In: Applications of Statistics and Probability in Civil Engineering - Proceedings of the 10th International Conference on Applications of Statistics and Probability, ICASP10; 2007:1-8.
7. Goda K, Hong H. Spatial correlation of peak ground motions and response spectra. *Bull Seismol Soc Am*. 2008;98(1):354-365.
8. Goda K, Atkinson G. Probabilistic characterization of spatially correlated response spectra for earthquakes in Japan. *Bull Seismol Soc Am*. 2009;99(5):3003-3020.
9. Goda K, Atkinson G. Intraevent spatial correlation of ground-motion parameters using SK-net data. *Bull Seismol Soc Am*. 2010;100(6):3055-3067.
10. Hong H, Zhang Y, Goda K. Effect of spatial correlation on estimated ground-motion prediction equations. *Bull Seismol Soc Am*. 2009;99(2A):928-934.
11. Jayaram N, Baker J. Correlation model for spatially distributed ground-motion intensities. *Earthq Eng Struct Dyn*. 2009;38(15):1687-1708.
12. Goda K. Interevent variability of spatial correlation of peak ground motions and response spectra. *Bull Seismol Soc Am*. 2011;101(5):2522-2531.
13. Esposito S, Iervolino I. Spatial correlation of spectral acceleration in European data. *Bull Seismol Soc Am*. 2012;102(6):2781-2788.
14. Sokolov V, Wenzel F, Wen K, Jean W. On the influence of site conditions and earthquake magnitude on ground-motion within-earthquake correlation: analysis of PGA data from TSMIP (Taiwan) network. *Bull Earthq Eng*. 2012;10(5):1401-1429.
15. Du W, Wang G. Intra-Event spatial correlations for cumulative absolute velocity, Arias intensity, and spectral accelerations based on regional site conditions. *Bull Seismol Soc Am*. 2013;103(2A):1117-1129.
16. Loth C, Baker J. A spatial cross-correlation model of spectral accelerations at multiple periods. *Earthq Eng Struct Dyn*. 2013;42(3):397-417.
17. Sokolov V, Wenzel F. Spatial correlation of ground motions in estimating seismic hazards to civil infrastructure. In: *Handbook of Seismic Risk Analysis and Management of Civil Infrastructure Systems*; 2013.
18. Sokolov V, Wenzel F. Further analysis of the influence of site conditions and earthquake magnitude on ground-motion within-earthquake correlation: Analysis of PGA and PGV data from the K-NET and the KiK-net (Japan) networks. *Bull Earthq Eng*. 2013;11(6):1909-1926.
19. Wang G, Du W. Spatial cross-correlation models for vector intensity measures (PGA, Ia, PGV, and SAs) considering regional site conditions. *Bull Seismol Soc Am*. 2013;103(6):3189-3204.
20. Weatherill G, Silva V, Crowley H, Bazzurro P. Exploring the impact of spatial correlations and uncertainties for portfolio analysis in probabilistic seismic loss estimation. *Bull Earthq Eng*. 2015;13(4):957-981.
21. Markhvida M, Ceferino L, Baker J. Modeling spatially correlated spectral accelerations at multiple periods using principal component analysis and geostatistics. *Earthq Eng Struct Dyn*. 2018;47(5):1107-1123.
22. Chen Y, Baker J. Spatial correlations in CyberShake physics-based ground-motion simulations. *Bull Seismol Soc Am*. 2019;109(6):2447-2458.
23. Heresi P, Miranda E. Uncertainty in intraevent spatial correlation of elastic pseudo-acceleration spectral ordinates. *Bull Earthq Eng*. 2019;17(3):1099-1115.
24. Baker J, Chen Y. Ground motion spatial correlation fitting methods and estimation uncertainty. *Earthq Eng Struct Dyn*. 2020;49(15):1662-1681.
25. Kuehn N, Abrahamson N. Spatial correlations of ground motion for non-ergodic seismic hazard analysis. *Earthq Eng Struct Dyn*. 2020;49(1):4-23.

26. Schiappapietra E, Douglas J. Modelling the spatial correlation of earthquake ground motion: Insights from the literature, data from the 2016–2017 Central Italy earthquake sequence and ground-motion simulations. *Earth-Science Rev*. 2020;203:103139.
27. Schiappapietra E, Douglas J. Assessment of the uncertainty in spatial-correlation models for earthquake ground motion due to station layout and derivation method. *Bull Earthq Eng*. 2021;19, 5415-5438
28. Chen Y, Bradley B, Baker J. Nonstationary spatial correlation in New Zealand strong ground-motion data. *Earthq Eng Struct Dyn*. 2021; 50: 3421-3440.
29. Du W, Ning C. Modeling spatial cross-correlation of multiple ground motion intensity measures (SAs, PGA, PGV, Ia, CAV, and significant durations) based on principal component and geostatistical analyses. *Earthq Spectra*. 2021;37(1):486-504.
30. Infantino M, Smerzini C, Lin J. Spatial correlation of broadband ground motions from physics-based numerical simulations. *Earthq Eng Struct Dyn*. 2021;50(10):2575-2594.
31. Schiappapietra E, Smerzini C. Spatial correlation of broadband earthquake ground motion in Norcia (Central Italy) from physics-based simulations. *Bull Earthq Eng*. 2021;19(12):4693-4717.
32. Bastías N, Montalva G. Chile strong ground motion flatfile. *Earthq Spectra*. 2016;32(4):2549-2566.
33. Abrahamson N. Statistical properties of peak ground accelerations recorded by the SMART 1 array (Taiwan). *Bull Seismol Soc Am*. 1988;78(1):26-41.
34. Jayaram N, Baker J. Statistical tests of the joint distribution of spectral acceleration values. *Bull Seismol Soc Am*. 2008;98(5):2231-2243.
35. Montalva G, Bastías N, Rodriguez-Marek A. Ground-motion prediction equation for the Chilean subduction zone. *Bull Seismol Soc Am*. 2017;107(2):901-911.
36. Abrahamson N, Youngs R. A stable algorithm for regression analyses using the random effects model. *Bull Seismol Soc Am*. 1992;82(1):505-510.
37. Candia G, Poulos A, de la Llera J, Crempien J, Macedo J. Correlations of spectral accelerations in the Chilean subduction zone. *Earthq Spectra*. 2020;36(2):788-805.
38. Zerva A, Zervas V. Spatial variation of seismic ground motions: an overview. *Applied Mechanics Reviews*. 2002;55(3):271-297.
39. der Kiureghian A. A coherency model for spatially varying ground motions. *Earthq Eng Struct Dyn*. 1996;25(1):99-111.
40. Wang D, Mori J. Frequency-dependent energy radiation and fault coupling for the 2010 Mw8.8 Maule, Chile, and 2011 Mw9.0 Tohoku, Japan, earthquakes. *Geophys Res Lett*. 2011;38(22).
41. Kiser E, Ishii M. The 2010 Mw 8.8 Chile earthquake: triggering on multiple segments and frequency-dependent rupture behavior. *Geophys Res Lett*. 2011;38(7). https://doi.org/10.1029/2011GL047140
42. Ruiz S, Madariaga R, Astroza M, et al. Short-period rupture process of the 2010 Mw 8.8 Maule Earthquake in Chile. *Earthq Spectra*. 2012;28(SUPPL.1):1-18.

How to cite this article: Aldea S, Heresi P, Pastén C. Within-event spatial correlation of peak ground acceleration and spectral pseudo-acceleration ordinates in the Chilean subduction zone. *Earthquake Engng Struct Dyn*. 2022;1–16. https://doi.org/10.1002/eqe.3674